Rethinking Vertical Transport of Buoyant Plastics in Open Channels

Charuni Wickramarachchi[1], Felipe Condo[1], Robert K. Niven[1], and Matthias Kramer[1]

[1]UNSW Canberra, School of Engineering and Technology, Canberra, ACT 2610, Australia

This manuscript is a non–peer-reviewed preprint that has been submitted to EarthArXiv. The paper is currently under consideration for publication in a peer-reviewed journal.

Key Points:

- The Rouse profile is not universally applicable to buoyant plastics due to the influence of surface tension effects
- Our analytical and numerical results suggest previous experimental data may not have reached convergence
- The proposed Surface-Detachment Rouse chart predicts the transport regimes of buoyant plastics

Corresponding author: Matthias Kramer, m.kramer@unsw.edu.au

Abstract
Recent studies have demonstrated that the vertical distribution of positively buoyant plastic particles in turbulent open channel flows can be described by a modified Rouse profile. However, implicit observations in the literature also suggest that floating particles remain confined to the air–water interface due to surface tension forces. To shed more light on this apparent contradiction, we analytically and numerically develop an expression for the minimum development length, the streamwise distance required to achieve converged concentration profiles, revealing that previous studies may have not reached this critical distance. Building on this, we develop a regime map that integrates free surface detachment and bed entrainment processes with the Rouse profile, providing a comprehensive framework to predict the transport modes of both positively and negatively buoyant plastics in open channel flows. We anticipate that this framework will enhance the understanding and prediction of plastic pollution dynamics in riverine environments, ultimately supporting more effective monitoring and mitigation strategies.

1 Introduction

The distribution and behavior of plastic particles in aquatic environments have become crucial areas of research due to the widespread issue of plastic pollution. A key question in understanding plastic transport and distribution in riverine systems is whether negatively and positively buoyant plastics follow traditional sediment transport models, such as the Rouse equation.

The Rouse equation provides a theoretical solution to the advection-diffusion equation for sediment transport in water and has been widely used to estimate the vertical distribution of suspended sediment concentrations (Rouse, 1937). The resulting Rouse profile is based on several key assumptions: (i) the flow is two-dimensional, steady, and uniform, with the streamwise velocity representing the dominant flow direction; (ii) the time-averaged vertical velocity is zero, although instantaneous vertical fluctuations are nonzero; and (iii) suspended particles are diffusively transported from regions of high to low concentration until equilibrium is achieved between the downward flux due to gravitational settling (deposition) and the upward flux due to turbulent diffusion (entrainment) (Dey, 2014).

Since the Rouse equation was developed to describe the behaviour of suspended sediment, it implicitly assumes that particles are denser than water. This allows for interaction between settling particles and the bed boundary, with continuous exchange between the bed load and suspended load under equilibrium conditions. Such exchange is facilitated by lift forces capable of re-entraining settled particles into the flow. In contrast, plastic densities typically range between 0.85 and 1.41 kg/m^3 (Gent et al., 2009; Mark, 2009; Grigorescu et al., 2019), meaning that plastic particles can be either positively or negatively buoyant. To account for this, we present a modified Rouse equation derived for both positively and negatively buoyant particles (§ Appendix A)

$$\frac{\overline{c}}{\overline{c}_{\mathrm{ref}}} = \left(\frac{\frac{H}{z_{\mathrm{ref}}} - 1}{\frac{H}{z} - 1} \right)^{\beta_p}, \tag{1}$$

where $\overline{c}$ is the plastic concentration, $\overline{c}_{\mathrm{ref}}$ is a reference concentration, H is the water depth, z_{ref} is the reference elevation, z is the vertical coordinate, and $\beta_p = w_t/(\kappa u_*)$ is a modified Rouse number, with w_t being the particle's terminal velocity, u_* the shear velocity, and κ the Van Kármán coefficient.

It is important to note that in the modified Rouse equation (Equation 1), w_t is taken as positive for rising particles and negative for settling particles, an inversion of the convention used in Rouse's original work (Rouse, 1961). Here, we argue that this formulation provides a more consistent and unified framework for describing the vertical transport of plastic particles in aquatic environments. Figure 1 illustrates an example application of Equation

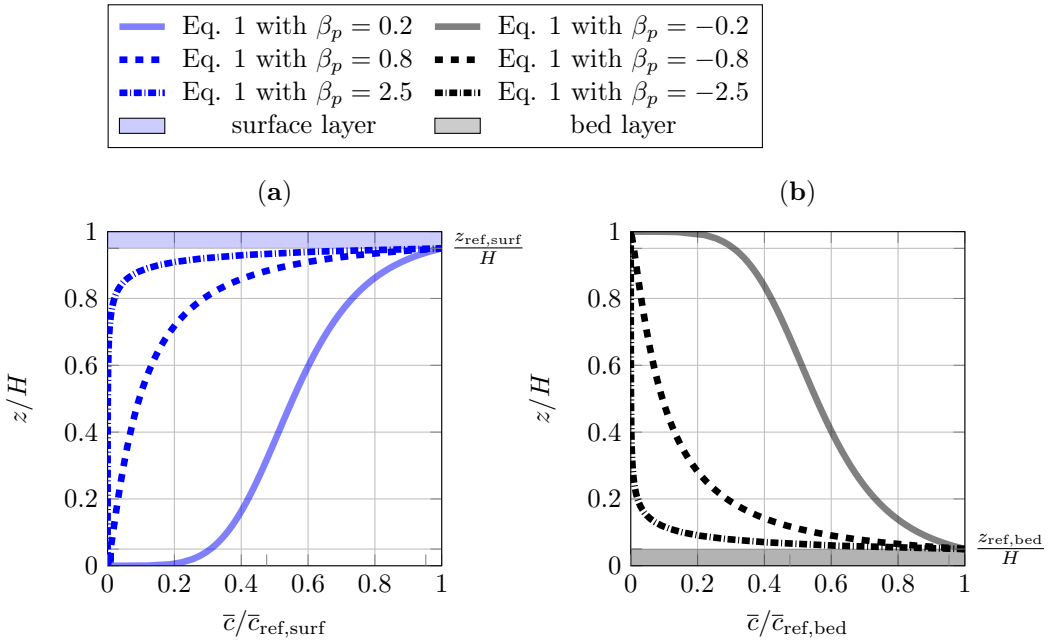

Figure 1. Modified Rouse profile for (**a**) positively buoyant plastic particles with a reference level $z_{\mathrm{ref,surf}}/H = 0.95$; (**b**) negatively buoyant plastic particles with a reference level $z_{\mathrm{ref,bed}}/H = 0.05$

1 for both positively and negatively buoyant plastic particles, where the reference level for the surface layer was set to $z_{\mathrm{ref,surf}}/H = 0.95$, and for the bed layer to $z_{\mathrm{ref,bed}}/H = 0.05$. So far, Equation 1, or comparable formulations, has also been applied in the literature to characterize the vertical distribution of positively buoyant plastics in several studies, including Cowger et al. (2021) and Wright et al. (2022).

However, it is important to note that neither the conceptual work of Cowger et al. (2021) nor the numerical implementation by Wright et al. (2022) account for surface tension forces, which can entrap particles at the air–water interface and thereby inhibit exchange between the surface layer and the suspended layer. This physical mechanism has been highlighted in recent studies, including Valero et al. (2022) and Kramer (2025). As such, we hypothesize that the Rouse profile **may not apply universally** to positively buoyant plastics, due to the restricted vertical exchange imposed by surface tension effects. This finding has important implications for plastic transport monitoring as well as for the design of capturing strategies targeting buoyant plastic debris at the water surface.

Our hypothesis is supported by several implicit observations in experimental studies from the literature, which are briefly discussed below. Alsina et al. (2020) released floating particles at the free surface of a wave tank and observed that "*within the experimental conditions, floating particles do not detach from the free surface showing a large influence of the particle positive buoyancy*". Zaat (2020) performed flume experiments with HDPE sheets and reported that "*releasing of plastic at the water surface did not result in mixing at all. Sheets would remain at the surface due to surface tension*". Finally, Born et al. (2023) released particles into an open-channel flume and observed that floating particles "*remained at the water surface, even at the intense inlet turbulence caused by the discharge entering the flume from the pump*".

These observations collectively suggest that floating particles tend to remain at the water surface, even under turbulent conditions, which raises the question of whether true equilibrium conditions were achieved in studies that experimentally observed a Rouse profile,

such as those of Valero et al. (2022). Notably, this reported that plastic samples were overconcentrated in the near-surface layers, primarily due to surface tension effects, which were strong enough to hold the plastics captive at the free surface.

In the present work, we aim to determine whether the Rouse profile applies to positively buoyant plastics and identify the conditions under which it holds. To achieve this, we derive an analytical solution for the minimum development length (§ 2.1), which represents the minimum flume length required to achieve converged and reliable concentration results, enabling us to assess whether previous experiments were sufficiently long to accurately model plastic transport processes. Our formulation is based on the Rouse number, water depth, release position, and bed roughness. To account for turbulence effects, we perform Lagrangian Transport Simulations of an idealized two-dimensional open-channel flume, which help evaluate the vertical distribution of particles under controlled turbulence conditions (§ 2.2). This approach permits us to extend our analytical solution to account for these flow dynamics. Following the establishment of the minimum development length, we compare our results with experimental studies from the literature (§ 3), and we develop a preliminary regime map delineating the conditions under which the Rouse profile is expected to hold for positively and negatively buoyant plastics (§ 4).

2 Methods

2.1 Analytical Solution for Minimum Development Length

In this section, we derive an analytical expression for the minimum development length $L_{\min}$, defined as the shortest horizontal distance a particle must travel to reach the surface in the absence of diffusion, as illustrated in Figure 2. It is assumed that a particle is released at a dimensionless elevation $\zeta = z_{\text{source}}/H$, and that its horizontal transport is governed by the depth-averaged velocity above the particle's initial height. This effective velocity is given by $\langle\overline{u}\rangle_{(1-\zeta)} = \frac{1}{(1-\zeta)H}\int_{z=\zeta H}^{H}\overline{u}\,\mathrm{d}z$, where the operator $\langle\cdot\rangle$ denotes depth-averaging.

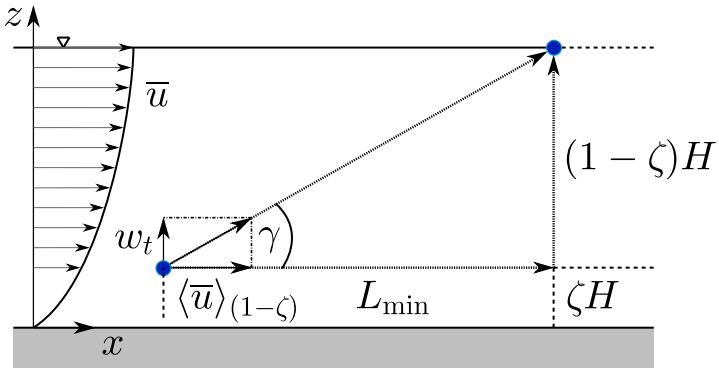

Figure 2. Determination of the minimum required development length for experiments on plastic concentration profiles; note that the release position of the particle is given as $z_{\text{source}} = \zeta H$.

The angle γ between the horizontal advection velocity $\langle\overline{u}\rangle_{(1-\zeta)}$ and the particle rise velocity w_t (Figure 2) can be written as

$$\tan(\gamma) = \frac{(1-\zeta)\,H}{L_{\min}} = \frac{w_t}{\langle\overline{u}\rangle_{(1-\zeta)}}, \tag{2}$$

which can be rearranged to give an expression for the dimensionless minimum development length

$$\frac{L_{\min}}{H} = \frac{(1-\zeta)\,\langle \overline{u} \rangle_{(1-\zeta)}}{w_t}. \tag{3}$$

We now assume that the streamwise velocity profile follows the classical log-law

$$\overline{u}(z) = \frac{u_*}{\kappa} \ln\left(\frac{z}{z_0}\right), \tag{4}$$

where $\overline{u}$ is the time-averaged streamwise velocity, u_* is the shear velocity, κ (= 0.41) is the van Karman coefficient, z_0 is the roughness height, and z is the vertical coordinate. Inserting this profile into the definition of the depth-averaged velocity above the particle's initial height, and performing the integration, yields

$$\begin{aligned} \langle \overline{u} \rangle_{(1-\zeta)} &= \frac{1}{(1-\zeta)\,H} \frac{u_*}{\kappa} \int_{\zeta H}^{H} \ln\left(\frac{z}{z_0}\right) \mathrm{d}z \\ &= \frac{1}{(1-\zeta)} \frac{u_*}{\kappa} \left[\ln\left(\frac{H}{z_0}\right) - \zeta \ln\left(\frac{\zeta H}{z_0}\right) - (1-\zeta) \right]. \end{aligned} \tag{5}$$

Combining this with Equation 3 leads to the final analytical solution for the dimensionless minimum development length

$$\frac{L_{\min}}{H} = \frac{1}{\beta_p} \frac{1}{\kappa^2} \left(\ln\left(\frac{H}{z_0}\right) - \zeta \ln\left(\frac{\zeta H}{z_0}\right) - (1-\zeta) \right), \tag{6}$$

where $\beta_p = w_t/(\kappa u_*)$ is the modified Rouse number, and κ is the von Kármán constant. This derivation is based on several simplifying assumptions. The flow is considered steady, fully developed, and unidirectional, with a streamwise velocity profile that follows the classical logarithmic law of the wall. The particle is assumed to be passive, and its vertical motion is governed solely by a constant rise velocity w_t, implying that vertical diffusion is neglected.

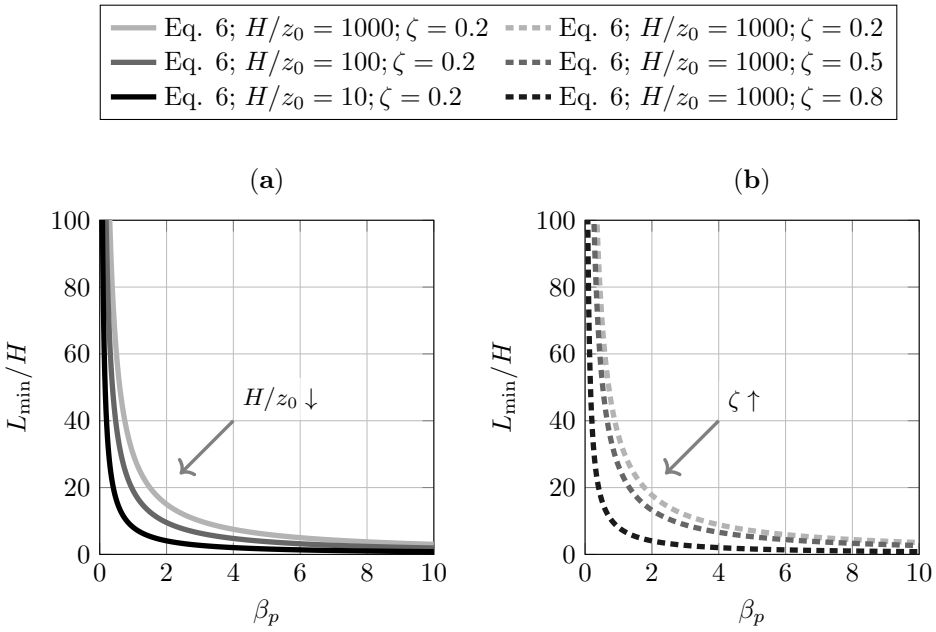

Figure 3. Minimum development lengths evaluated using Equation 6: (**a**) Effects of increasing bottom roughness; (**b**) Effects of increasing release height.

Physically, Equation 6 shows that the minimum development length increases with decreasing modified Rouse number, reflecting situations where the particle rises more slowly

(small w_t) or the flow is faster (large $\langle\overline{u}\rangle$). The effect of bed roughness enters through z_0, which shapes the velocity profile and thus the horizontal transport of the particle. Particles released deeper in the flow (smaller ζ) have farther to rise and are carried farther downstream. The impact of these processes on the dimensionless development lengths is illustrated in Figure 3.

2.2 Lagrangian Transport Simulations

In our work, we simulate the transport of positively buoyant plastic spheres within a two-dimensional open channel flume using a Random Walk Model. This stochastic approach extends the analytical solution for the minimum development length, given in Equation 6, by accounting for vertical diffusion, which is neglected in the purely advective case. The water depth in the simulation is $H = 0.3$ m, and the flow is described by a logarithmic velocity profile, that is, Equation 4. For the simulation, we used $u_* = 0.021$ m/s, and $z_0 = 3 \cdot 10^{-4}$ m, corresponding to a hydraulically rough bed with $H/z_0 = 1000$. These parameters resulted in a depth-averaged mean velocity of $\langle\overline{u}\rangle = \int_{z=0}^{H} \overline{u}\,\mathrm{d}z = 0.3$ m/s. The selected conditions closely match those used in previous laboratory studies (Valero et al., 2022), enabling direct comparison and validation of our numerical results.

Particle motion is governed by its position vector $\mathbf{x}_p$, with the particle velocity defined by the time derivative

$$\frac{\mathrm{d}\mathbf{x}_p}{\mathrm{d}t} = \mathbf{u}_p, \tag{7}$$

where t denotes the time, the subscript p refers a plastic particle, and $\mathbf{u}_p$ is the velocity vector of the point particle relative to an inertial frame of reference. Equation 7 can be reformulated using a Random Walk Model. We adopt the scheme proposed by Visser (1997), which has been successfully applied in previous studies (Nordam et al., 2019, 2023; Wickramarachchi et al., 2024). This model accounts for both advective and diffusive transport, described as follows

$$x_p(t+\Delta t) = x_p(t) \; + \; \overbrace{\overline{u}\,\Delta t}^{\text{advection step}} \; + \; \overbrace{\frac{\partial \mathcal{D}_x}{\partial x}\Delta t + \mathcal{R}\sqrt{2\Delta t \mathcal{D}_x^*}}^{\text{diffusion step}}, \tag{8}$$

$$z_p'(t+\Delta t) = z_p(t) \; + \; (\overline{w} + w_t)\Delta t \; + \; \frac{\partial \mathcal{D}_z}{\partial z}\Delta t + \mathcal{R}\sqrt{2\Delta t \mathcal{D}_z^*}. \tag{9}$$

In these expressions, x_p and z_p represent the horizontal and vertical components of the particle position vector $\mathbf{x}_p$. The superscript $'$ in Equation 9 indicates an intermediate step that is subsequently corrected to satisfy boundary conditions (e.g., particle reflection at the bed or absorption at the free surface). The time step is denoted by Δt. The terms $\overline{u}$ and $\overline{w}$ correspond to the time-averaged advection velocities in the horizontal and vertical directions, respectively, with vertical flow velocities neglected in this model ($\overline{w} \approx 0$). The turbulent diffusivities in the horizontal and vertical directions are denoted by $\mathcal{D}_x$ and $\mathcal{D}_z$, where for simplicity, we assume $\mathcal{D}_x \approx 0$, and $\mathcal{D}_z$ follows established open-channel flow relationships (Dey, 2014)

$$\mathcal{D}_z = \kappa u_* z \left(1 - \frac{z}{H}\right). \tag{10}$$

The terms $\mathcal{D}_x^*$ and $\mathcal{D}_z^*$ are the local diffusivities evaluated at intermediate positions, defined as $x^* = x_p + \frac{\partial \mathcal{D}_x}{\partial x}\frac{\Delta t}{2}$ and $z^* = z_p + \frac{\partial \mathcal{D}_z}{\partial z}\frac{\Delta t}{2}$. Here, $\frac{\partial \mathcal{D}_x}{\partial x} \approx 0$, and $\frac{\partial \mathcal{D}_z}{\partial z} = \kappa u_* \left(1 - \frac{2z}{H}\right)$. The parameter $\mathcal{R}$ is a normally distributed random number with zero mean and unit standard deviation, and w_t is the terminal rise velocity of the positively buoyant plastic. These velocities are selected so that that the modified Rouse number $\beta_p = w_t/(\kappa u_*)$ takes

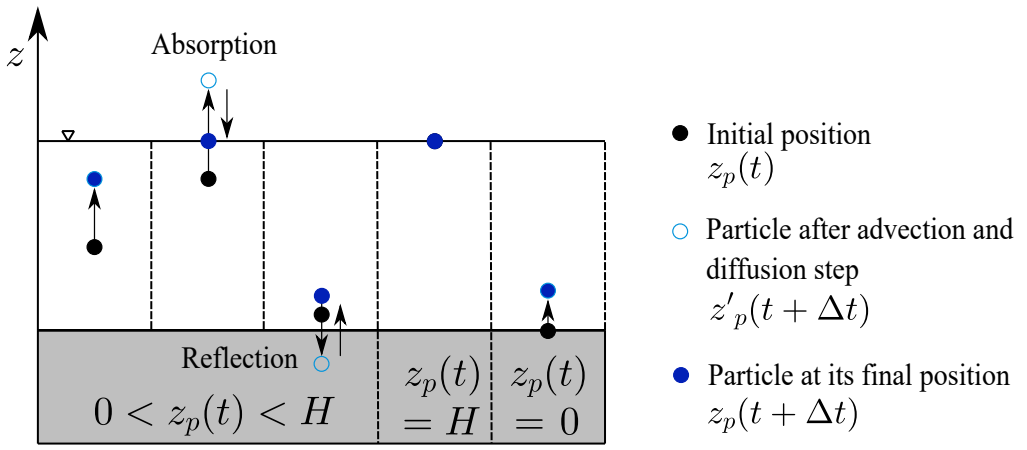

Figure 4. Illustration of implemented boundary conditions, including absorptive surface boundary and reflective bed boundary.

values ranging from 0.5 to 10, in increments of 0.5. Note that this approach does not necessarily require the selection of a particle diameter. However, as an example, assuming a plastic density of $\rho_p = 950$ kg/m^3 and applying the settling velocity formulation of Ferguson and Church (2004), the corresponding particle diameters range between approximately 0.4 mm $< D_p <$ 5.6 mm. Both the assumed density and the resulting diameter range are consistent with the particle properties used in the experiments of Born et al. (2023).

As the simulation domain is unbounded in the streamwise direction, boundary conditions are applied only in the vertical (z) direction, accounting for particle–bed and particle–surface interactions. Based on literature evidence indicating that floating particles do not detach once they reach the free surface, the surface treated as an absorbing boundary, as exemplified in Figure 4. This implementation is further supported by the discussion on the shear velocity required for detachment (see Section 4). In contrast, the channel bed is modelled as a reflective boundary; however, interactions with the bed are rare due to the positive buoyancy of the particles. Mathematically, the boundary conditions are applied through an intermediate step, denoted as z'_p, which is subsequently corrected to ensure particles remain within the physical domain. The implementation proceeds as follows

$$z'_p(t+\Delta t) = \begin{cases} z_p(t) + (\overline{w} + w_t)\Delta t + \dfrac{\partial \mathcal{D}_z}{\partial z}\Delta t + \mathcal{R}\sqrt{2\Delta t \mathcal{D}_z^*} & \text{if } 0 < z_p(t) < H, \\ H & \text{if } z_p(t) = H, \\ \left| (\overline{w} + w_t)\Delta t + \dfrac{\partial \mathcal{D}_z}{\partial z}\Delta t + \mathcal{R}\sqrt{2\Delta t \mathcal{D}_z^*} \right| & \text{if } z_p(t) = 0. \end{cases} \tag{11}$$

$$z_p(t+\Delta t) = \begin{cases} z'_p(t+\Delta t) & \text{if } 0 \le z'_p(t+\Delta t) \le H, \\ H & \text{if } z'_p(t+\Delta t) > H, \quad \text{(absorptive boundary)} \\ -z'_p(t+\Delta t) & \text{if } z'_p(t+\Delta t) < 0. \quad \text{(reflective boundary)} \end{cases} \tag{12}$$

Equations 11 and 12 ensure accurate representation of particle dynamics near the boundaries, maintaining physical consistency throughout the simulation. An illustration of the implemented boundary conditions is shown in Figure 4.

3 Results

3.1 Particle Trajectories and Surface Interactions

Using the Random Walk Model as described, we performed a total of 60 simulations. In each run, we simulated the trajectories of 10,000 positively buoyant plastic particles across a range of modified Rouse numbers, from 0.5 to 10 in increments of 0.5, at three different release positions: $\zeta = 0.2, 0.5$, and 0.8. The time step was $\Delta t = 0.1$ s, which is in accordance with previously established (Rossman & Boulos, 1996; Gräwe et al., 2012). For each case, we tracked the length travelled by each particle before surfacing, enabling a statistical characterization of particle arrival distances. Figure 5**a** shows exemplary trajectories of twenty particles, released at $\zeta = 0.2$, with a modified Rouse number of $\beta_p = 5$. The corresponding probability density function (PDF) of arrival distances is presented in Figure 5**b**.

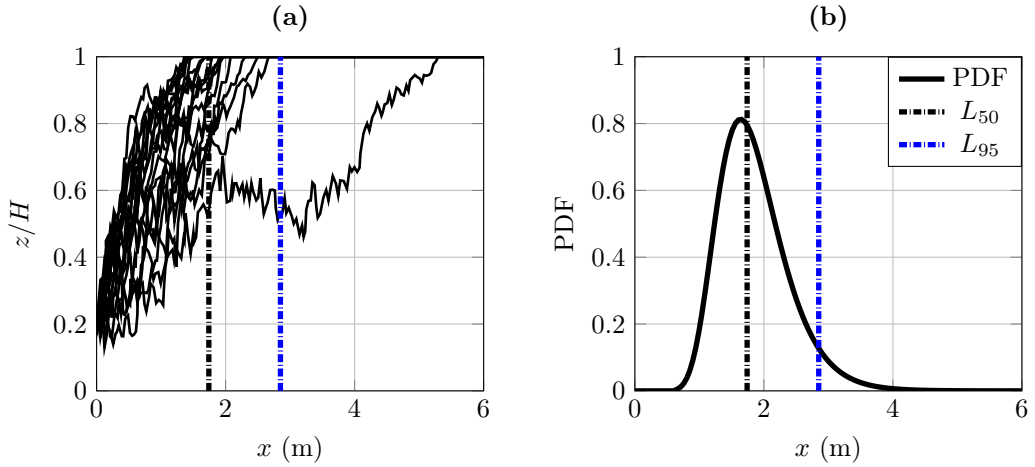

Figure 5. Numerical simulation results for $\beta_p = 5$: (**a**) Selected trajectories of twenty particles; (**b**) Probability density function of surface arrival distances, with L_{50} and L_{95} indicating the 50th and 95th percentiles, respectively.

Arrival distances follow a lognormal distribution, and percentiles of this distribution, such as the 50th and 95th percentiles, are used to characterize the development lengths, corresponding to the median (L_{50}) and near-maximum expected arrival distances (L_{95}), respectively (Figure 5**b**).

A comparison of the development lengths obtained from the 60 simulations with the analytical solution (Equation 6) is presented in Figure 6 for the three different release heights. A strong agreement is observed between $L_{\min}$ and L_{50}, that is $L_{\min} \approx L_{50}$, implying that the development length of particles transported without turbulence is similar to the median distance travelled by particles reaching the surface under turbulent conditions. This indicates that, on average, turbulence does not significantly alter the typical median transport distance of positively buoyant particles, which is primarily governed by buoyant rise and mean flow advection.

In contrast, the development length L_{95} is significantly larger than L_{50} (Figure 6), reflecting the influence of turbulence in increasing the spread of particle arrival distances

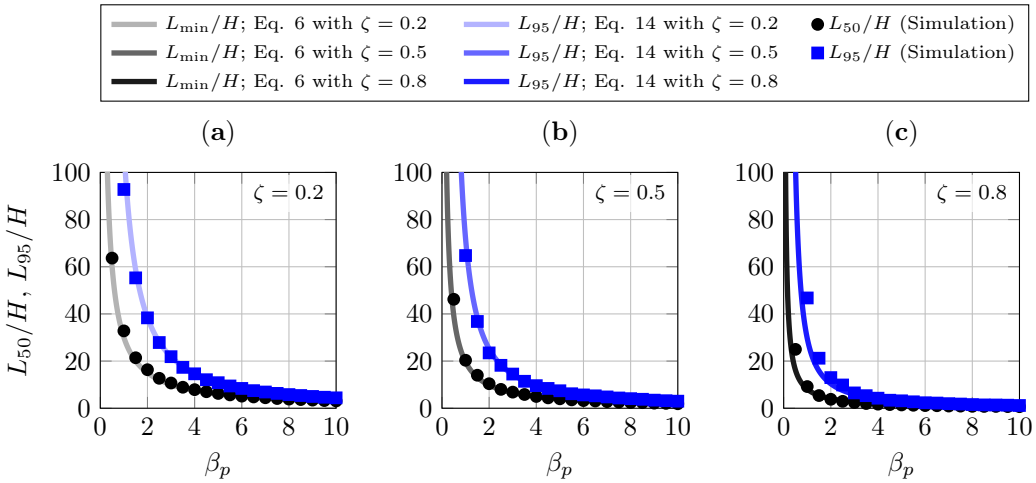

Figure 6. Comparison of analytical versus simulated development lengths for different release heights; the ratio of water depth to bottom roughness is $H/z_0 = 1000$: (**a**) $\zeta = 0.2$; (**b**) $\zeta = 0.5$; and (**c**) $\zeta = 0.8$.

and causing some particles to travel much farther before surfacing. This occurs because, in turbulence-dominated regimes ($\beta_p < 1$), vertical turbulent transport overwhelms the particle's rise velocity, making their motion largely random and allowing even positively buoyant plastics to remain submerged for extended distances. In contrast, when advection dominates ($\beta_p > 1$), particle trajectories become predictable, with buoyant particles inevitably rising to the surface, explaining the minimal deviation between turbulent and non-turbulent cases at high Rouse numbers.

For practical purposes, L_{95} is more important than L_{50}, because it represents near-maximum expected development length. When designing flume experiments, using L_{95} as benchmark for the development length ensures that the physical domain is sufficiently long to capture the full range of particle behaviour, including the delayed arrival of particles influenced by turbulence. This is essential for ensuring that turbulence effects are properly represented and that results are statistically converged.

To build on the comparison between analytical and numerical development lengths, we now seek a practical means of incorporating turbulent effects into the analytical framework. While the minimum development length $L_{\min} \approx L_{50}$, as per Equation 6, provides a lower bound for particle surfacing under purely advective transport, it does not account for the dispersion introduced by turbulence. In particular, the significantly larger values of L_{95} highlight the importance of accounting for the tail of the distribution of arrival distances when designing experiments.

We now define a correction factor $\Omega(\beta_p, \zeta) = L_{95}/L_{50}$, which captures turbulence-induced increase in the effective development length. Figure 7 shows the variation of Ω with respect to the modified Rouse number β_p. Since the influence of the release height ζ on Ω is relatively small, we simplify the correction factor to depend primarily on β_p. The relationship can be approximated by the empirical formula

$$\Omega = \frac{L_{95}}{L_{50}} \approx 3.7102\, \beta_p^{-0.416} \tag{13}$$

valid for $0.2 \lesssim \beta_p \leq 10$. Combining Equation 13 with Equation 6 yields an expression for the dimensionless L_{95}

$$\frac{L_{95}}{H} = \frac{\Omega}{\beta_p} \frac{1}{\kappa^2} \left(\ln\left(\frac{H}{z_0}\right) - \zeta \ln\left(\frac{\zeta H}{z_0}\right) - (1-\zeta) \right). \tag{14}$$

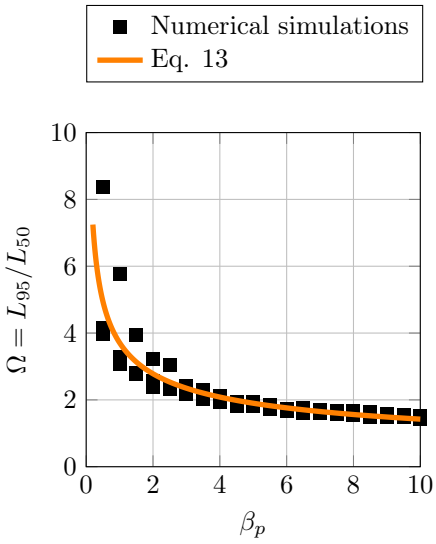

Figure 7. Correction factor Ω versus modified Rouse number β_p

This expression, which has also been plotted previously in Figure 6, captures the extended development length due to turbulence effects and will be used in the following section to examine the experimental design of previous studies.

3.2 Comparison of Development Length with Prior Studies

Here, we are comparing our analytical expressions, Equations 6 and 14, with previous flume experiments. In Figure 8, dimensionless flume lengths L_{50}/H and L_{95}/H are plotted against the actual experimental conditions of Zaat (2020), Valero et al. (2022), and Born et al. (2023) on the ordinate, which allows us to assess whether the experiments fulfilled the minimum requirements. As discussed in the previous section, L_{95} is more important for practical purposes, and it is seen that the majority of the experiments from Zaat (2020) and Valero et al. (2022) may not have converged, while the experiments of Born et al. (2023) fall to the left of the 1:1 line, indicating that the flume length was sufficient in those cases (Figure 8**b**). Overall, our findings imply that conclusions drawn from experiments with insufficient flume lengths should be treated with caution, as incomplete development could compromise the accuracy and representativeness of plastic transport observations.

4 Discussion

4.1 Surface Detachment-Rouse chart

To consolidate our study, we are developing a regime map that integrates free surface detachment and bed entrainment processes with the Rouse profile. This map delineates the dominant plastic transport modes and identifies the conditions under which the Rouse profile remains valid for both positively and negatively buoyant plastics, across a range of flow regimes and particle characteristics. The regime map can be interpreted in two complementary ways: as a Surface Detachment–Rouse chart, which emphasizes surface detachment thresholds and plastic transport modes, and as a Shields–Rouse diagram, which highlights bed entrainment thresholds and transport regimes.

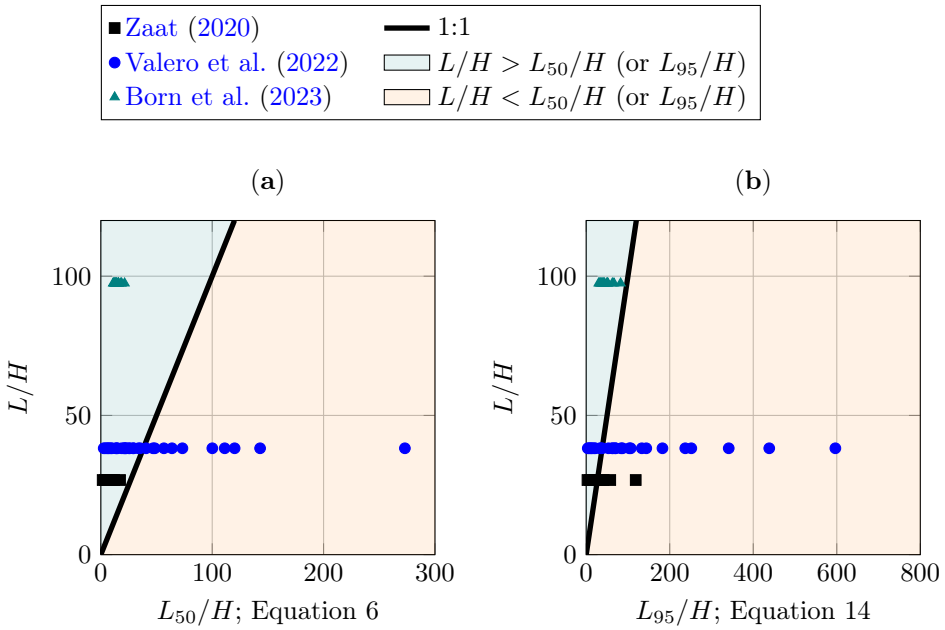

Figure 8. Comparison of analytical expressions for the development length versus previous studies: (**a**) L_{50}; (**b**) L_{95}.

Equation (15), derived by Kramer (2025), defines the critical surface detachment parameter for positively buoyant plastics. It relates the dimensionless critical shear velocity u_* required to detach particles from the surface to key flow and particle properties

$$\Theta_{\mathrm{cr},p} = \frac{u_{*,\mathrm{cr}}^2}{\left(\frac{\rho_w - \rho_p}{\rho_w}\right) g D_p} = \frac{9.17\,\Gamma_{\mathrm{cr}}}{\alpha_p\, C_{D,F_w}}, \tag{15}$$

where $\Theta_{\mathrm{cr},p}$ is the dimensionless shear velocity at surface detachment (referred to as surface detachment parameter), and the subscript "cr" denotes a critical threshold. Here, D_p is the sphere volume-equivalent plastic diameter, g is the gravitational acceleration, ρ_w and ρ_p are the water and plastic densities respectively. Γ_{cr} is a plastic-based Bond number at detachment (see § Appendix B), and C_{D,F_w} is a drag coefficient associated with the turbulent downpull force F_w, as defined in Valero et al. (2022) and Kramer (2024). The parameter $\alpha_p = A_{\mathrm{proj}} D_p / \mathcal{V}_p$ is a shape factor, where A_{proj} is the projected area of the particle parallel to the streamwise flow direction and $\mathcal{V}_p$ is the particle volume. Note that Equation (15) is expressed in squared form compared to the original formulation in Kramer (2025), in order to align dimensionally with the classical Shields parameter. Additionally, the assumption $\rho_w > \rho_p$ implies that this formulation is specifically valid for positively buoyant plastics.

To represent Equation (15) in our Surface Detachment–Rouse chart, we first define a reference particle, analogous to how natural sediment is used in the classical Shields diagram, to normalize flow and particle properties. We select a spherical plastic particle as the reference and assume that its diameter corresponds to the median grain size of the underlying sediment, that is, $D_p = d_{50}$. This assumption maintains consistency between the two diagrams and provides a standardized basis for our analysis; the influence of varying particle shapes and sizes is addressed subsequently.

To construct the surface detachment curves, we proceed as follows: First, we select a particle size corresponding to a specified diameter d_{50}, as well as a particle density ρ_p. Next, we evaluate Equation (15), where the shape factor is taken as $\alpha_p = 1.5$, corresponding to a spherical particle. We also assume $C_{D,F_w} = 5$, which represents a conservative estimate for

the turbulent drag coefficient acting on buoyant plastics in natural flow conditions. With these parameters, we compute $\Theta_{\mathrm{cr},p,d_{50}}$, where the subscript d_{50} indicates that this value corresponds to our reference particle. Having computed $\Theta_{\mathrm{cr},p,d_{50}}$, we evaluate the critical shear velocity using $u_{*,\mathrm{cr}} = \left(\Theta_{\mathrm{cr},p,d_{50}} \left(\frac{\rho_w - \rho_p}{\rho_w}\right) g D_p\right)^{0.5}$, which is simply a re-arrangement of Equation (15). Finally, we evaluate the shear Reynolds number as $Re_* = (u_{*,\mathrm{cr}} d_{50})/\nu_w$, where ν_w is the kinematic viscosity of water. An example calculation illustrating this procedure is provided in § Appendix B and is included in Figure 9**a**.

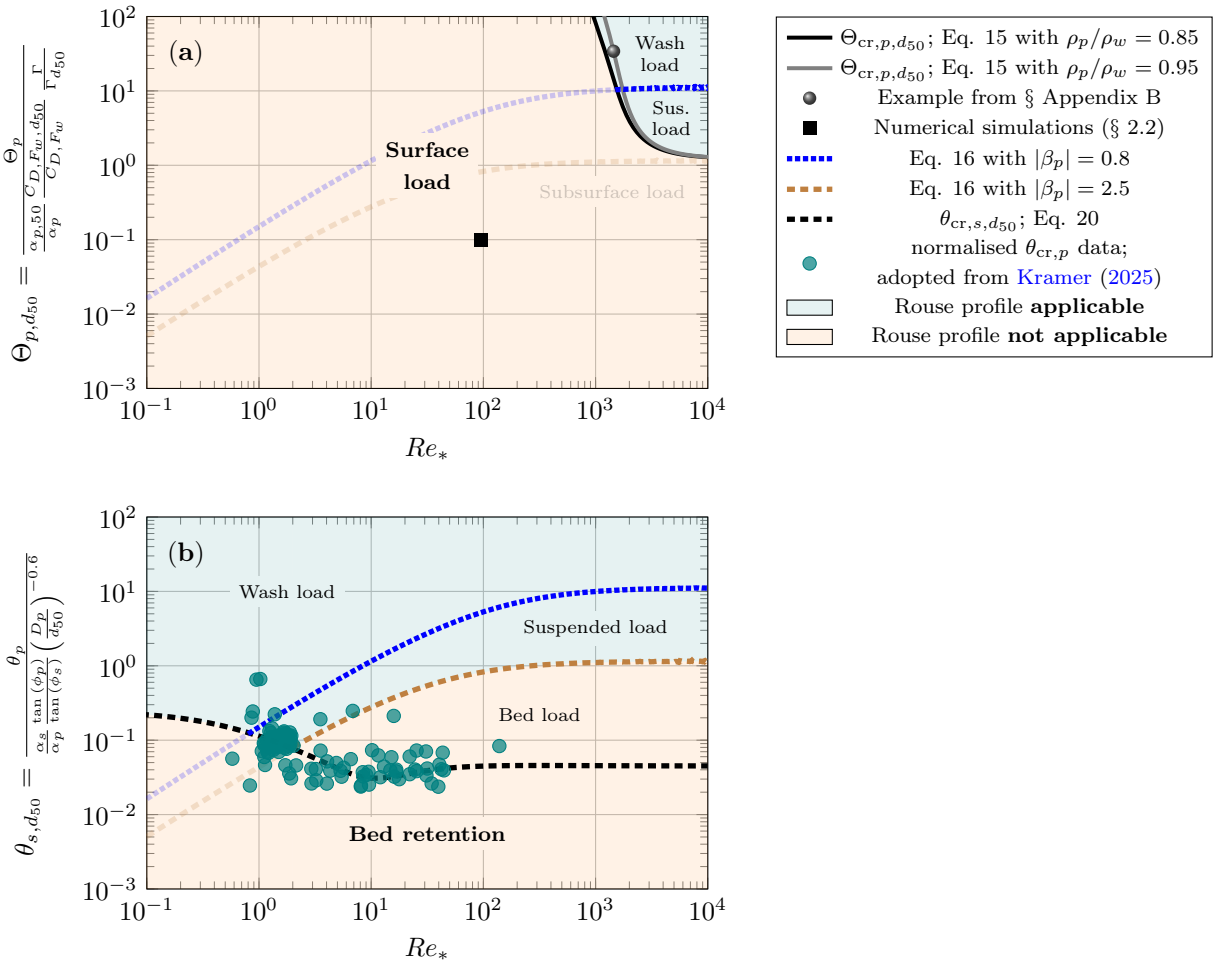

Figure 9. Regime maps for plastic transport in fluvial systems: (**a**) Surface Detachment-Rouse chart for positively buoyant plastics; the reference particle is a spherical plastic with $D_p = d_{50}$; (**b**) Shields-Rouse diagram for negatively buoyant plastics; the reference particle is a sediment particle with $D_s = d_{50}$.

Figure 9**a** shows the results of this analysis, where we have plotted the surface detachment curves for two different densities, that is, $\rho_p/\rho_w = 0.85$ and $\rho_p/\rho_w = 0.95$, which are representative of typical values for commercially available positively buoyant plastics. It is noted that the density term appears on both sides of Equation (15) due to the normalization scheme adopted from the classical Shields formulation. As a result, a slight dependence on plastic density is retained. However, this dependence is relatively small, as illustrated in Figure 9**a**. More importantly, we observe that the vast majority of positively buoyant plastics remain entrapped at the surface (i.e., in the surface load regime) under typical flow conditions. This behaviour aligns with the absorptive boundary condition incorporated into our Lagrangian transport simulation, which is explicitly shown in Figure 9**a**. Only under

relatively high shear velocities, and with larger particle sizes, do particles detach from the free surface. This suggests that surface load is the dominant transport mode for small, buoyant plastic particles. For reference, the critical surface detachment parameter exceeds $\Theta_{\mathrm{cr},p,d_{50}} > 100$ for particles smaller than $d_{50} < 3.09$ mm in Figure 9**a**.

Table 1. Comparison of plastic transport modes for settling and rising particles with typical Shields parameter and Rouse number ranges

Transport Mode	θ_p (-), Θ_p (-)	β_p (-)	Interpretation
	Settling Particles ($\beta_p < 0$)		
Bed retention	$\theta_p < \theta_{\mathrm{cr},p}$	N/A	Particles remain immobile
Bed load	$\theta_p \approx \theta_{\mathrm{cr},p}$	$\beta_p \ll -2.5$	Particles travel predominantly at the river bed
Suspended load	$\theta_p > \theta_{\mathrm{cr},p}$	$-2.5 < \beta_p < -0.8$	Particles intermittently lifted
Wash load	$\theta_p \gg \theta_{\mathrm{cr},p}$	$\beta_p > -0.8$	Turbulence keeps particles fully suspended
	Rising Particles ($\beta_p > 0$)		
Wash load	$\Theta_p \gg \Theta_{\mathrm{cr},p}$	$\beta_p < 0.8$	Turbulence keeps particles fully suspended
Suspended load	$\Theta_p > \Theta_{\mathrm{cr},p}$	$0.8 < \beta_p < 2.5$	Particles intermittently detached
Subsurface load	$\Theta_p \approx \Theta_{\mathrm{cr},p}$	$\beta_p \gg 2.5$	Particles travel predominantly at the surface
Surface load	$\Theta_p < \Theta_{\mathrm{cr},p}$	N/A	Particles become entrapped at the surface

To illustrate other transport modes, we added curves of constant Rouse numbers β_p to our plot, as defined by Equation 16

$$\frac{u_*^2}{\left(\frac{|\rho_w-\rho_p|}{\rho_w}\right) g\, d_{50}} = \left(-\sqrt{\frac{0.75\, C_2\, Re_*^2}{4\, C_1^2}} + \sqrt{\frac{0.75\, C_2\, Re_*^2}{4\, C_1^2} + \frac{Re_*}{\kappa\, C_1}\frac{1}{|\beta_p|}}\right)^2, \tag{16}$$

which was adopted from Pekker (2017) to account for positively and negatively buoyant plastics. Here, C_1 and C_2 are empirical coefficients that describe particle drag behavior in the Stokes and Newton regimes, respectively, with typical values of $C_1 = 18$ and $C_2 = 0.4$ for smooth spheres (Ferguson & Church, 2004). Equation (16) was incorporated into Figure 9 to provide a more comprehensive regime classification, with typical β_p ranges for different transport modes, such as wash load, suspended load, and others, summarized in Table 1.

As discussed previously, we constructed the Surface Detachment-Rouse chart for spherical reference particles with $D_p = d_{50}$. To account for variations in particle shape and size, we relate the surface detachment parameters of an arbitrary plastic particle to those of the reference particle by expressing

$$\frac{\Theta_p}{\Theta_{p,d_{50}}} = \frac{\alpha_{p,50}}{\alpha_p}\frac{C_{D,F_w,d_{50}}}{C_{D,F_w}}\frac{\Gamma}{\Gamma_{d_{50}}}, \tag{17}$$

which leads to the following normalization of Θ_p

$$\Theta_{p,d_{50}} = \frac{\Theta_p}{\frac{\alpha_{p,50}}{\alpha_p}\frac{C_{D,F_w,d_{50}}}{C_{D,F_w}}\frac{\Gamma}{\Gamma_{d_{50}}}}. \tag{18}$$

This normalization enables us to adjust the detachment parameter for plastics of varying shapes and sizes, thereby extending the regime map's applicability beyond spherical reference particles to a wide range of plastic particle geometries and dimensions. Note that a similar approach was proposed by Kramer (2025) for bed entrainment, who demonstrated that the classical Shields diagram for natural sediments can be applied to plastics by expressing the plastic Shields parameter θ_p as

$$\theta_{s,d_{50}} = \frac{\theta_p}{\frac{\alpha_s}{\alpha_p}\frac{\tan(\phi_p)}{\tan(\phi_s)}\left(\frac{D_p}{d_{50}}\right)^{-0.6}}, \tag{19}$$

where the subscript s refers to sediment, and d_{50} denotes the reference sediment particle diameter $D_s = d_{50}$. The form of the plastic Shields parameter is analogous to that for natural sediments, and is given by Kramer (2025) $\theta_p = u_*^2 / \left(\left(\frac{\rho_p - \rho_w}{\rho_w}\right) g D_p\right)$, assuming $\rho_p > \rho_w$. In the context of bed entrainment, the shape factor α_p includes the projected area of the particle taken perpendicular to the flow direction. The friction coefficient ϕ accounts for particle–bed interactions: ϕ_p represents the friction coefficient between the plastic particle and the underlying sediment, while ϕ_s represents the friction between a sediment particle and the sediment bed. The corresponding Shields-Rouse diagram for negatively buoyant plastics is shown in Figure 9**b**, where the threshold for motion is given by an empirical correlation

$$\theta_{\mathrm{cr},s,d_{50}} = 0.165(Re_* + 0.6)^{-0.8} + 0.045\,\exp(-40\,Re_*^{-1.3}), \tag{20}$$

which was proposed by Sui et al. (2021). For completeness, normalized critical plastic Shields parameters $\theta_{\mathrm{cr},p}$ from Kramer (2025) are also included in Figure 9**b**.

In summary, this section has developed a comprehensive regime map that integrates surface detachment, bed entrainment, and the Rouse profile to classify plastic transport modes across a range of particle properties and flow conditions. By normalizing key parameters for different particle shapes and sizes, we extended classical sediment transport frameworks to plastics with varying buoyancies. The green and orange shaded areas in Figure 9 illustrate the parameter space where the Rouse profile provides a valid description of vertical plastic concentration distributions for positively and negatively buoyant particles, respectively. While the Rouse profile appears broadly applicable for negatively buoyant plastics, its applicability for positively buoyant plastics seems more limited, primarily due to the dominant influence of surface tension forces acting on small particles. This finding carries important implications for plastic surface monitoring strategies, which are further discussed in the next section. Overall, the regime map offers a valuable framework for understanding and predicting plastic transport dynamics in fluvial environments.

4.2 Limitations and Implications

While the proposed framework provides a useful basis for understanding plastic transport in fluvial systems, several limitations should be acknowledged

- Hydrodynamic simplifications: Our analysis does not account for waves and windage. While we anticipate that these processes are generally negligible in open-channel flows, they may be important in estuarine or coastal environments.
- Surface boundary condition: We applied an absorptive boundary in the Lagrangian transport simulation, corresponding to the orange shaded region in Figure 9**a**. This assumes irreversible surface entrapment.
- Assumed drag coefficient: In the absence of direct measurements, we adopted a constant turbulent drag coefficient of $C_{D,F_w} = 5$. While conservative, this assumption requires experimental validation for improved accuracy.
- Reference particle geometry: Spherical particles were selected as a reference in the Surface Detachment–Rouse chart. This offers a reasonable first approximation, and shape effects are addressed through normalization. However, the detachment formulation may require revision for open-shaped or flexible particles, such as cups or films.

- Effective density assumption: Our proposed framework incorporates *effective particle properties*, including modified density due to processes such as fragmentation, degradation, and bio-fouling. While this provides flexibility, it assumes that such modifications are known or can be reasonably estimated.

Our findings have several important implications for understanding plastic transport in fluvial systems. Most notably, our results challenge earlier conclusions by Cowger et al. (2021), who postulated that positively buoyant particles follow the Rouse profile without accounting for surface tension effects. They also differ from those of Zaat (2020) and Valero et al. (2022), where reported concentration profiles may not have reached convergence due to insufficient flume lengths (Figure 8**b**).

The presented Surface Detachment–Rouse chart (Figure 9**a**) highlights that the majority of positively buoyant particles are transported as surface load, suggesting that surface monitoring may be sufficient to capture the bulk of buoyant plastic transport under typical flow conditions. However, this conclusion is sensitive to hydrodynamic conditions and particle properties, as certain conditions can lead to surface detachment (Figure 9**a**).

In addition, the developed Shields–Rouse diagram (Figure 9**b**) shows that negatively buoyant plastics are often transported as suspended load or wash load, which requires subsurface or depth-integrated sampling strategies to accurately quantify transport. Overall, our findings emphasize the importance of adapting monitoring approaches to the prevailing plastic types and local flow regimes, as a one-size-fits-all strategy may lead to substantial over- or underestimations of total plastic flux.

5 Conclusion

This study highlights the complex interactions between turbulent mixing and interfacial forces that govern the vertical distribution of buoyant plastics in open channel flows. By developing an analytical and numerical expression for the minimum development length, we show that previous experimental investigations may not have fully met the streamwise distance required for plastics to reach an equilibrium vertical concentration profile. The introduction of a regime map integrating free surface detachment and bed entrainment processes with the modified Rouse profile provides a unified framework to predict the transport behaviour of both positively and negatively buoyant plastics. These insights are critical for improving the accuracy of plastic transport models and for designing effective sampling and mitigation strategies in riverine environments. Future work should focus on validating this framework across a range of flow conditions and particle properties to deepen our understanding of the physical processes controlling plastic transport and to refine predictive models of buoyant particle behaviour in riverine environments.

Acknowledgments
The authors thank Dr Daniel Valero for fruitful discussion. The use of the AI language model ChatGPT (OpenAI) for assistance in revising small portions of the manuscript's grammar is acknowledged. All content, scientific interpretations, and conclusions remain the sole responsibility of the authors.

Notation

The following symbols are used in this paper:

Latin Symbols

A_{proj}	projected area	(m^2)
c	instantaneous plastic concentration	(kg m^{-1})
$\overline{c}$	time-averaged plastic concentration	(kg m^{-1})
c'	plastic concentration fluctuation	(kg m^{-1})
C_1, C_2	empirical coefficients describing particle drag	(-)
D_{D,F_w}	drag coefficient for downpull force	(-)
d_{50}	median grain size of underlying sediment	(m)
D_p	sphere volume-equivalent plastic diameter	(m)
D_s	sphere volume-equivalent sediment diameter	(m)
$\mathcal{D}_m$	molecular diffusivity	($\text{m}^2\ \text{s}^{-1}$)
$\mathcal{D}_x$	turbulent streamwise diffusivity	($\text{m}^2\ \text{s}^{-1}$)
$\mathcal{D}_x^*$	turbulent streamwise diffusivity at intermediate position x^*	($\text{m}^2\ \text{s}^{-1}$)
$\mathcal{D}_z$	turbulent vertical diffusivity	($\text{m}^2\ \text{s}^{-1}$)
$\mathcal{D}_z^*$	turbulent vertical diffusivity at intermediate position z^*	($\text{m}^2\ \text{s}^{-1}$)
F_B	buoyancy force	(N)
F_W	weight force	(N)
F_w	downpull force	(N)
F_σ	surface tension force	(N)
$\mathcal{K}$	integration constant	(-)
g	gravitational acceleration	(m s^{-2})
h_w	submerged particle depth	(m)
H	water depth	(m)
L_{min}	minimum development length	(m)
L_{50}	median development length	(m)
L_{95}	near maximum development length	(m)
L_σ	contact length for surface tension	(m)
Re_*	shear Reynolds number	(-)
$\mathcal{R}$	random number with zero mean and unit standard deviation	(-)
t	time	(s)
u	instantaneous streamwise water velocity	(m s^{-1})
$\overline{u}$	time-averaged streamwise water velocity	(m s^{-1})
u'	fluctuating streamwise water velocity	(m s^{-1})
$\langle\overline{u}\rangle$	depth-averaged streamwise velocity	(m s^{-1})
u_*	bed shear velocity	(m s^{-1})
$\mathbf{u}_p$	particle velocity vector	(m s^{-1})
$\mathcal{V}_p$	particle volume	(m^3)
$\mathcal{V}_{p,w}$	submerged particle volume	(m^3)
w	instantaneous vertical water velocity	(m s^{-1})
$\overline{w}$	time-averaged vertical water velocity	(m s^{-1})
w'	fluctuating vertical water velocity	(m s^{-1})
w_t	terminal particle velocity	(m s^{-1})
x	streamwise coordinate	(m)
x_p	streamwise particle position	(m)
$\mathbf{x}_p$	particle position vector	(m)
z	vertical coordinate	(m)
z_0	roughness height	(m)
z_p	vertical particle position	(m)
z_p'	intermediate particle position for boundary condition	(m)

Greek Letters

α_p	plastic shape factor	(-)
β_p	$= w_t/(\kappa u_*)$; plastic Rouse number	(-)
γ	angle between advection and particle rise velocity	(°)
Γ	plastic-based Bond number	(-)

Δt	simulation timestep	(s)
ζ	dimensionless elevation	(-)
θ_p	plastic Shields parameter	(-)
θ_s	sediment Shields parameter	(-)
Θ_p	plastic surface detachment parameter	(-)
κ	van Karman coefficient	(-)
ν	kinematic viscosity	(m^2 s^{-1})
ρ	density	(kg m^{-3})
σ	surface tension	(N m^{-1})
ϕ_p	friction coefficient between plastic and sediment bed	(-)
ϕ_s	friction coefficient between sediment particle and sediment bed	(-)
Ψ	contact angle	(°)
Ω	correction factor for L_{95}	(-)

Indices and Operators

bed	channel bed
cr	critical
d_{50}	d_{50} corresponds to reference
max	maximum
p	plastic particle
ref	reference
s	sediment
source	plastic source
surf	free surface
w	water

Appendix A Modified Rouse Profile for Plastics in Water

We start with the 2-dimensional advection-diffusion equation for plastics in water,

$$\frac{\partial c}{\partial t} + \left[\frac{\partial (u\,c)}{\partial x} + \frac{\partial (w\,c)}{\partial z}\right] = \mathcal{D}_m \left[\frac{\partial^2 c}{\partial x^2} + \frac{\partial^2 c}{\partial z^2}\right], \tag{A1}$$

where transverse transport is neglected. Here, c is the instantaneous plastic concentration, x, and z are the streamwise and vertical coordinates with associated velocities u and w, and $\mathcal{D}_m$ is the molecular diffusivity. Introducing Reynolds averaging with $c = \overline{c} + c'$, $u = \overline{u} + u'$, and $w = \overline{w} + w'$ yields

$$\frac{\partial \overline{c}}{\partial t} + \overline{u}\frac{\partial \overline{c}}{\partial x} + \overline{w}\frac{\partial \overline{c}}{\partial z} = \underbrace{-\frac{\partial \overline{u'c'}}{\partial x} - \frac{\partial \overline{w'c'}}{\partial z}}_{\text{covariance terms}} + \mathcal{D}_m \left[\frac{\partial^2 \overline{c}}{\partial x^2} + \frac{\partial^2 \overline{c}}{\partial z^2}\right], \tag{A2}$$

where the operators $\overline{\ }$ and $'$ denote the time-averaged and the fluctuating component, respectively. Next, we relate turbulent mass flux through concentration gradients using turbulent diffusivities $\mathcal{D}$

$$\overline{u_i' c'} = -\mathcal{D}\frac{\partial \overline{c}}{\partial x_i}, \tag{A3}$$

noting that turbulent diffusivities are typically much larger than molecular diffusivities, i.e., $\mathcal{D} \gg \mathcal{D}_m$, we neglect $\mathcal{D}_m$ in a first approximation. Thus, Equation A2 can be written as

$$\frac{\partial \overline{c}}{\partial t} + \overline{u}\frac{\partial \overline{c}}{\partial x} + \overline{w}\frac{\partial \overline{c}}{\partial z} = \frac{\partial}{\partial x}\left(\mathcal{D}_x \frac{\partial \overline{c}}{\partial x}\right) + \frac{\partial}{\partial z}\left(\mathcal{D}_z \frac{\partial \overline{c}}{\partial z}\right). \tag{A4}$$

A governing equation for the vertical distribution of plastics in water can be formulated by assuming steady-state conditions and neglecting horizontal changes, i.e., $\partial(\cdot)/\partial t = 0$, and

$\partial(\cdot)/\partial x = 0$, leading to

$$\frac{\partial(\overline{w}\,\overline{c})}{\partial z} = \frac{\partial}{\partial z}\left(\mathcal{D}_z \frac{\partial \overline{c}}{\partial z}\right). \tag{A5}$$

Integrating Equation A5 in vertical (z) direction

$$\int \frac{\partial}{\partial z}\left(\overline{w}\,\overline{c}\right) \mathrm{d}z = \int \frac{\partial}{\partial z}\left(\mathcal{D}_z \frac{\partial \overline{c}}{\partial z}\right) \mathrm{d}z \tag{A6}$$

leads to

$$\overline{w}\,\overline{c} = \mathcal{D}_z \frac{\partial \overline{c}}{\partial z} + \mathcal{K}, \tag{A7}$$

where $\mathcal{K}$ is an integration constant. Rearranging gives

$$\frac{1}{\overline{c}}\,\mathrm{d}\overline{c} = \frac{\overline{w}}{\mathcal{D}_z}\,\mathrm{d}z, \tag{A8}$$

where we have replaced the partial differential by the total differential, and $\mathcal{K} = 0$ is taken. Assuming that the time-averaged vertical velocity corresponds to the particle's terminal velocity $\overline{w} = w_t$, a second integration from a reference level z_{ref} to an arbitrary elevation z gives

$$\int_{\overline{c}=\overline{c}_{\mathrm{ref}}}^{\overline{c}=\overline{c}(z)} \frac{1}{\overline{c}}\,\mathrm{d}\overline{c} = w_t \int_{z=z_{\mathrm{ref}}}^{z} \frac{1}{\mathcal{D}_z}\mathrm{d}z, \tag{A9}$$

which can be simplified

$$\frac{\overline{c}}{\overline{c}_{\mathrm{ref}}} = \exp\left(w_t \int_{z=z_{\mathrm{ref}}}^{z} \frac{1}{\mathcal{D}_z}\mathrm{d}z\right). \tag{A10}$$

Now, we invoke a parabolic distribution of turbulent diffusivity

$$\mathcal{D}_z = \kappa u_* z\left(1 - \frac{z}{H}\right), \tag{A11}$$

where u_* is the shear velocity, and H is the water depth. Substitution and subsequent integration gives

$$\frac{\overline{c}}{\overline{c}_{\mathrm{ref}}} = \exp\left(\frac{w_t}{\kappa\, u_*} \ln\left[\frac{\frac{H}{z_{\mathrm{ref}}} - 1}{\frac{H}{z} - 1}\right]\right), \tag{A12}$$

which can be simplified to

$$\frac{\overline{c}}{\overline{c}_{\mathrm{ref}}} = \left(\frac{\frac{H}{z_{\mathrm{ref}}} - 1}{\frac{H}{z} - 1}\right)^{\beta_p}, \tag{A13}$$

where $\beta_p = \frac{w_t}{\kappa\, u_*}$ is the modified Rouse number for plastics in water. In this definition, w_t is taken as positive when directed upward (for rising, positively buoyant particles) and negative when directed downward (for settling, negatively buoyant particles). It is noted that the modified Rouse equation for plastics in water, i.e., Equation A13, differs from Rouse's original formulation, in which a negative sign was included in the derivation and the particle settling velocity was assumed to be positive.

In the context of plastic pollution research, a Rouse profile for positively buoyant particle was first presented by Cowger et al. (2021), where rising velocities were used with a negative sign. In contrast, the current formulation takes w_t as positive for rising particles and as negative for settling particles, which we believe provides a more consistent and intuitive framework for describing vertical plastic transport.

Appendix B Worked Example for Surface Detachment Curve Construction

In this appendix, we provide a detailed example calculation to illustrate the procedure for constructing surface detachment curves for buoyant plastic particles in open channel

flows. Using a reference particle size d_{50} and particle density ρ_p, we demonstrate how to evaluate the critical surface parameter $\Theta_{\mathrm{cr},p,d_{50}}$ based on Equation (15). Let us assume a particle with $D_p = d_{50} = 0.005$ m and $\rho_p = 950$ kg/m^3. We further assume a drag coefficient $C_{D,F_w} = 5$, which is a conservative estimate for buoyant plastics in turbulent flow, and we consider the particle to be spherical. For a sphere, the shape factor α_p is given by the ratio of projected area times diameter to particle volume. This results in

$$\alpha_p = \frac{A_{\mathrm{proj}} D_p}{\mathcal{V}_p} = \frac{\left(\frac{\pi}{4} D_p^2\right) D_p}{\frac{\pi}{6} D_p^3} = \frac{\frac{\pi}{4} D_p^3}{\frac{\pi}{6} D_p^3} = \frac{\frac{\pi}{4}}{\frac{\pi}{6}} = 1.5. \tag{B1}$$

Next, we consider the plastic-based Bond number, denoted as Γ_{cr}, at the point of detachment. It is defined as the ratio of the net vertical forces acting on the particle to the maximum buoyant weight difference, given by Kramer (2025)

$$\Gamma_{\mathrm{cr}} = \frac{(F_B)_{\mathrm{cr}} - F_W + (F_\sigma)_{\mathrm{cr}}}{|F_{B,\max} - F_W|} = \frac{\rho_w\, g\, (\mathcal{V}_{p,w})_{\mathrm{cr}} - \rho_p\, g\, \mathcal{V}_p + (L_\sigma)_{\mathrm{cr}}\, \sigma \sin(\Psi)}{g\, \mathcal{V}_p\, |\rho_w - \rho_p|}. \tag{B2}$$

Here, F_B is the buoyancy force acting on the particle, F_W is the particle weight, and F_σ represents the surface tension force acting along the air-water-particle contact line. The parameters ρ_w and ρ_p are the densities of water and the particle, respectively, while g is the acceleration due to gravity. The variable $\mathcal{V}_p = \frac{\pi}{6} D_p^3 = 6.5450 \cdot 10^{-8}\,\mathrm{m}^3$ denotes the total volume of the particle, and $(\mathcal{V}_{p,w})_{\mathrm{cr}}$ is the critical submerged volume of the particle at detachment. The term $(L_\sigma)_{\mathrm{cr}}$ is the critical length associated with surface tension forces, $\sigma = 0.072$ N/m is the surface tension coefficient, and $\Psi = 105°$ is the contact angle. The particle's relative submergence at detachment, that is $(h_w/D_p)_{\mathrm{cr}}$, is given as 0.679 (Figure B1 in Kramer (2025)), so

$$h_{w,\mathrm{cr}} = 0.679 \cdot D_p = 0.0034\,\mathrm{m}. \tag{B3}$$

For a spherical particle, $(\mathcal{V}_{p,w})_{\mathrm{cr}}$ and $(L_\sigma)_{\mathrm{cr}}$ are related to $h_{\mathrm{cr},w}$ through (Kramer, 2025)

$$(\mathcal{V}_{p,w})_{\mathrm{cr}} = \frac{\pi\, h_{\mathrm{cr},w}^2}{3}(1.5 D_p - h_{\mathrm{cr},w}) = 4.9547 \cdot 10^{-8}\ \mathrm{m}^3, \tag{B4}$$

$$(L_\sigma)_{\mathrm{cr}} = 2\pi \sqrt{h_{\mathrm{cr},w}\, D_p - h_{\mathrm{cr},w}^2} = 0.0147\,\mathrm{m}. \tag{B5}$$

Substituting these values into Equation B2 gives

$$\begin{aligned}\Gamma_{\mathrm{cr}} &= \frac{1000 \cdot 9.81 \cdot 4.9547 \cdot 10^{-8} - 950 \cdot 9.81 \cdot 6.5450 \cdot 10^{-8} + 0.0147 \cdot 0.072 \cdot \sin(105°)}{9.81 \cdot 6.5450 \cdot 10^{-8} \cdot (1000 - 950)} \\ &= 27.9141.\end{aligned} \tag{B6}$$

This result is then used in Equation (15) to compute the critical surface detachment parameter

$$\Theta_{\mathrm{cr},p,d_{50}} = \frac{u_{*,\mathrm{cr}}^2}{\left(\frac{\rho_w - \rho_p}{\rho_w}\right) g\, D_p} = \frac{9.17\, \Gamma_{\mathrm{cr}}}{\alpha_p\, C_{D,F_w}} = \frac{9.17 \cdot 27.9141}{1.5 \cdot 5} = 34.1297. \tag{B7}$$

The critical shear velocity is

$$\begin{aligned}u_{*,\mathrm{cr}} &= \left(\Theta_{\mathrm{cr},p,d_{50}} \left(\frac{\rho_w - \rho_p}{\rho_w}\right) g D_p\right)^{0.5} \\ &= \left(34.1297 \cdot \left(\frac{1000 - 950}{1000}\right) \cdot 9.81 \cdot 0.005\right)^{0.5} = 0.2893\,\mathrm{m/s},\end{aligned} \tag{B8}$$

which corresponds to a shear Reynolds number of

$$Re_* = \frac{u_*\, d_{50}}{\nu_w} = \frac{0.2893 \cdot 0.005}{1 \cdot 10^{-6}} = 1446.6. \tag{B9}$$

The calculated pair of critical values, $Re_* = 1446.6$ and $\Theta_{\mathrm{cr},p,d_{50}} = 34.13$, characterizes the onset of particle detachment for the given buoyant plastic particle under the specified flow conditions (Figure 9**a**).

References

Alsina, J. M., Jongedijk, C. E., & van Sebille, E. (2020). Laboratory measurements of the wave-induced motion of plastic particles: influence of wave period, plastic size and plastic density. *Journal of Geophysical Research: Oceans*, *125*(12), e2020JC016294.

Born, M. P., Bruell, C., Schaefer, D., Hillebrand, G., & Schuettrumpf, H. (2023). Determination of microplastics' vertical concentration transport (rouse) profiles in flumes. *Environmental Science & Technology*, *57*(14), 5569–5579.

Cowger, W., Gray, A. B., Guilinger, J. J., Fong, B., & Waldschläger, K. (2021). Concentration depth profiles of microplastic particles in river flow and implications for surface sampling. *Environmental Science & Technology*, *55*(9), 6032–6041.

Dey, S. (2014). *Fluvial hydrodynamics*. Springer.

Ferguson, R., & Church, M. (2004). A simple universal equation for grain settling velocity. *Journal of sedimentary Research*, *74*(6), 933–937.

Gent, M. R., Menendez, M., Toraño, J., Isidro, D., & Torno, S. (2009). Cylinder cyclone (larcodems) density media separation of plastic wastes. *Waste Management*, *29*(6), 1819–1827.

Gräwe, U., Deleersnijder, E., Shah, S. H. A. M., & Heemink, A. W. (2012). Why the euler scheme in particle tracking is not enough: the shallow-sea pycnocline test case. *Ocean Dynamics*, *62*, 501–514.

Grigorescu, R. M., Grigore, M. E., Iancu, L., Ghioca, P., & Ion, R.-M. (2019). Waste electrical and electronic equipment: A review on the identification methods for polymeric materials. *Recycling*, *4*(3), 32.

Kramer, M. (2024). Considerations on free-surface detachment and bed entrainment of fluvial plastics. *arXiv preprint arXiv:2408.03081*.

Kramer, M. (2025). Surface detachment and bed entrainment of fluvial plastics. *Water Resources Research*, *61*(9).

Mark, J. E. (2009). Polymer data handbook.

Nordam, T., Kristiansen, R., Nepstad, R., & Röhrs, J. (2019). Numerical analysis of boundary conditions in a lagrangian particle model for vertical mixing, transport and surfacing of buoyant particles in the water column. *Ocean Modelling*, *136*, 107–119.

Nordam, T., Kristiansen, R., Nepstad, R., van Sebille, E., & Booth, A. M. (2023). A comparison of Eulerian and Lagrangian methods for vertical particle transport in the water column. *Geoscientific Model Development Discussions*, *2023*, 1–41.

Pekker, L. (2017). A calculator for sediment transport in microchannels based on the rouse number. *arXiv preprint arXiv:1712.07073*. Retrieved from `https://arxiv.org/abs/1712.07073`

Rossman, L. A., & Boulos, P. F. (1996). Numerical methods for modeling water quality in distribution systems: A comparison. *Journal of Water Resources planning and management*, *122*(2), 137–146.

Rouse, H. (1937). Modern conceptions of the mechanics of fluid turbulence. *Transactions of the American Society of Civil Engineers*, *102*(1), 463–505.

Rouse, H. (1961). *Fluid mechanics for hydraulic engineers*. Dover Publications,Inc. New York.

Sui, T., Staunstrup, L. H., Carstensen, S., & Fuhrman, D. R. (2021). Span shoulder migration in three-dimensional current-induced scour beneath submerged pipelines. *Coast. Engng.*, *164*.

Valero, D., Belay, B. S., Moreno-Rodenas, A., Kramer, M., & Franca, M. J. (2022). The key role of surface tension in the transport and quantification of plastic pollution in rivers. *Water research*, *226*, 119078.

Visser, A. W. (1997). Using random walk models to simulate the vertical distribution of particles in a turbulent water column. *Marine Ecology Progress Series*, *158*, 275–281.

Wickramarachchi, C., Niven, R. K., & Kramer, M. (2024). On the boundary conditions for lagrangian plastic transport models.

Wright, K., Hariharan, J., Passalacqua, P., Salter, G., & Lamb, M. P. (2022). From grains to

plastics: Modeling nourishment patterns and hydraulic sorting of fluvially transported materials in deltas. *Journal of Geophysical Research: Earth Surface*, *127*(11).

Zaat, L. (2020). Below the surface: A laboratorial research to the vertical distribution of buoyant plastics in rivers.